catalysts

MDPI

Article

CO_2 Reforming of CH_4 Using Coke Oven Gas over Ni/MgO-Al_2O_3 Catalysts: Effect of the MgO:Al_2O_3 Ratio

Ho-Ryong Park [1], Beom-Jun Kim [1], Yeol-Lim Lee [1], Seon-Yong Ahn [1], Kyoung-Jin Kim [1], Ga-Ram Hong [1], Seong-Jin Yun [1], Byong-Hun Jeon [2], Jong Wook Bae [3] and Hyun-Seog Roh [1,*]

1 Department of Environmental Engineering, Yonsei University, 1 Yonseidae-gil, Wonju 26493, Gangwon-do, Korea; phr19@yonsei.ac.kr (H.-R.P.); beomjunkim@yonsei.ac.kr (B.-J.K.); yllee@yonsei.ac.kr (Y.-L.L.); syahn99@yonsei.ac.kr (S.-Y.A.); kyoungjinkim@yonsei.ac.kr (K.-J.K.); hgr0108@yonsei.ac.kr (G.-R.H.); ysj9821@yonsei.ac.kr (S.-J.Y.)

2 Department of Earth Resources and Environmental Engineering, Hanyang University, 222 Wangsimni-ro, Seongdong-gu, Seoul 04763, Korea; bhjeon@hanyang.ac.kr

3 School of Chemical Engineering, Sungkyunkwan University (SKKU), 2066 Seobu-ro, Jangan-gu, Suwon 16419, Korea; finejw@skku.edu

* Correspondence: hsroh@yonsei.ac.kr

Abstract: Research is being actively conducted to improve the carbon deposition and sintering resistance of Ni-based catalysts. Among them, the Al_2O_3-supported Ni catalyst has been broadly studied for the dry reforming reaction due to its high CH_4 activity at the beginning of the reaction. However, there is a problem of deactivation due to carbon deposition of Ni/Al_2O_3 catalyst and sintering of Ni, which is a catalytically active material. Supplementing MgO in Ni/Al_2O_3 catalyst can result in an improved $MgAl_2O_4$ spinel structure and basicity, which can be helpful for the activation of methane and carbon dioxide molecules. In order to confirm the optimal supports' ratio in Ni/MgO-Al_2O_3 catalysts, the catalysts were prepared by supporting Ni after controlling the MgO:Al_2O_3 ratio stepwise, and the prepared catalysts were used for CO_2 reforming of CH_4 (CDR) using coke oven gas (COG). The catalytic reaction was conducted at 800 °C and at a high gas hourly space velocity (GHSV = 1,500,000 h^{-1}) to screen the catalytic performance. The Ni/MgO-Al_2O_3 (MgO:Al_2O_3 = 3:7) catalyst showed the best catalytic performance between prepared catalysts. From this study, the ratio of MgO:Al_2O_3 was confirmed to affect not only the basicity of the catalyst but also the dispersion of the catalyst and the reducing property of the catalyst surface.

Keywords: coke oven gas; CO_2 reforming of CH_4; MgO:Al_2O_3; support; reducibility; Ni dispersion; basicity

check for updates

Citation: Park, H.-R.; Kim, B.-J.; Lee, Y.-L.; Ahn, S.-Y.; Kim, K.-J.; Hong, G.-R.; Yun, S.-J.; Jeon, B.-H.; Bae, J.W.; Roh, H.-S. CO_2 Reforming of CH_4 Using Coke Oven Gas over Ni/MgO-Al_2O_3 Catalysts: Effect of the MgO:Al_2O_3 Ratio. *Catalysts* **2021**, *11*, 1468. https://doi.org/10.3390/catal11121468

Academic Editor: Antonio Vita

Received: 5 November 2021
Accepted: 29 November 2021
Published: 30 November 2021

1. Introduction

Since the adoption of the Paris Agreement on Climate Change in 2015, it has been necessary to put in place measures to cut down greenhouse gas emissions to limit the increase in the global average temperature to 1.5 °C relative to preindustrial levels [1,2]. To achieve the CO_2 levels required by the Paris Agreement, we must reach zero emissions by 2050 [1]. However, zeroing greenhouse gases is still difficult due to the following issues. First, as the population increases, energy consumption continues to increase [3,4]. Among them, fossil fuels account for 81% of the total energy consumption [5]. Second, some carbon-based resources are essential for industries, such as steel making, where high-temperature heat is required [6–8]. Copious amounts of by-product gas are generated in each unit process in the steel industry, which is the core industry of our society [9]. Greenhouse gas emissions in the form of by-products accounted for approximately 9% of global emissions from 1900 to 2015 [10]. The by-product gas of the steel industry is largely divided into coke oven gas (COG), which is generated in the process of producing coke by oxidizing coal in a coke oven, and CO_2 generated in a blast furnace when iron oxide is reduced to iron [11].

Coke oven gas, a representative steel by-product gas, contains approximately 27% methane (CH_4), which causes greenhouse gas problems when emitted (coke oven gas composition: CH_4: 28.0%, CO_2: 2.6%, CO: 8.0%, H_2: 55.6%, N_2: 5.8%) [12]. A steam-reforming reaction (SRM: $CH_4 + H_2O \rightarrow CO + 3H_2$) that can produce syngas from methane is being studied to utilize COG, but there are economic problems with the additional supply of steam [13,14].

The CO_2 reforming of CH_4 (CDR: $CH_4 + CO_2 \rightarrow 2CO + 2H_2$) has the advantage of using CH_4 and CO_2 as reactants to produce syngas, which is an elemental raw material with high added value [15]. In addition, the syngas produced by the dry reforming reaction (H_2:CO = 1:1) shows a favorable H_2:CO ratio for oxo compound synthesis compared to the syngas produced through the steam reforming reaction (H_2:CO = 3:1) [16]. However, as the dry reforming reaction proceeds at high temperatures above 700 °C, favorable conditions are formed for sintering of active metals and supports to occur, and catalyst deactivation may occur due to carbon deposition by methane decomposition [17]. In addition, the dry reforming reaction is a strong endothermic reaction, partially lowering the catalyst bed temperature and promoting the occurrence of the Boudouard reaction ($2CO \rightarrow C + CO_2$), causing carbon deposition on the catalyst surface, thereby deactivating the catalyst [18,19]. Therefore, to overcome these problems, it is necessary to develop a catalyst for dry reforming with high sintering and carbon deposition resistances.

Various studies have been conducted using noble metal (Ir, Rh, Ru, Pt, and Pd) catalysts, and strong sintering resistance and carbon deposition resistance have been demonstrated in the dry reforming reaction. However, there is a problem in entering the commercialization stage due to the low economic feasibility of the noble metal catalyst [20,21]. Therefore, although research on economical nickel (Ni)-based catalysts exhibiting excellent activity in dry reforming reactions is being actively conducted, the problem of catalyst deactivation due to the low sintering resistance and low carbon deposition resistance of Ni has become a major issue [22–26].

Research is being actively conducted to improve the catalyst deactivation problem of Ni-based catalysts. Out of them, the Al_2O_3-supported Ni catalyst has been broadly studied for the dry reforming reaction due to its high CH_4 activity at the beginning of the reaction [27–29].

However, there is a problem of deactivation due to carbon deposition of the Ni/Al_2O_3 catalyst and sintering of Ni, which is a catalytically active material [30].

Therefore, many studies have been conducted to improve the performance of Ni/Al_2O_3 catalysts. Alipour et al. reported that adding alkaline earth metal oxides (CaO or MgO), dopants can enhance the interaction between Ni and the Al_2O_3 support [31]. Sengupta et al. demonstrated that the surface basicity of the alkaline earth metal oxide can improve the activity of methane molecules, thereby alleviating the problem of carbon deposition in the catalyst during the dry reforming reaction [32]. Guo et al. found that $MgAl_2O_4$ can be used as a support for the dry reforming catalytic reaction of Ni because of its high melting point, good chemical stability, and low acidity [33].

Based on the studies outlined above, the supplementing of MgO in Ni/Al_2O_3 catalyst can result in an improved $MgAl_2O_4$ spinel structure and basicity, which can be helpful for the activation of CH_4 and CO_2 molecules.

In this study, Ni/MgO-Al_2O_3 catalysts prepared with different MgO:Al_2O_3 ratios were used with coke oven gas (COG) to compare their dry reforming performance (gas hourly space velocity (GHSV) = 1,500,000 h^{-1}) and to investigate how that performance relates to the characteristics of the catalysts. The correlations between the catalytic performance and the physicochemical properties were investigated.

2. Results and Discussion

MgO-Al_2O_3 was prepared by the one-step coprecipitation method with different MgO:Al_2O_3 ratios as a support. A Ni/MG catalyst was prepared by supporting a Ni precursor aqueous solution on the prepared MgO-Al_2O_3 support by the impregnation method, as shown in Scheme 1. Before chemisorption and CDR reaction, in situ reduction

was performed for 3 h at 800 °C. Prior to XRD and TEM analyses, ex situ reduction was carried out for 3 h at 800 °C, and passivation was conducted for 3 h at 25 °C (Scheme 1).

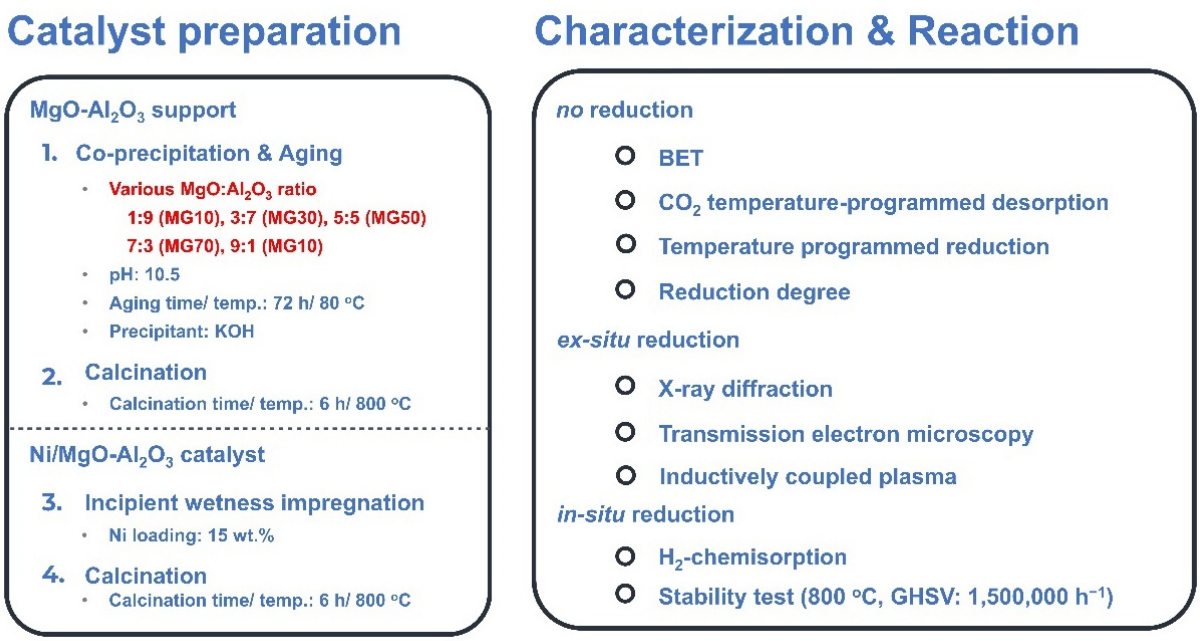

Scheme 1. Schematic of the preparation, characterization, and reaction conditions of the Ni/MG catalysts.

2.1. Catalyst Characterization

The BET surface areas (S.A.) of catalysts are listed in Table 1. The BET S.A. of the prepared MgO-Al_2O_3 support decreased as the MgO content increased and further decreased as Ni was loaded onto the MgO-Al_2O_3 support. As a result, the BET S.A. of the prepared Ni/MG catalyst was shown to have the following order: Ni/MG10 (139.2 m^2/g) > Ni/MG30 (120.8 m^2/g) > Ni/MG50 (104.2 m^2/g) > Ni/MG70 (104.0 m^2/g) > Ni/MG90 (76.6 m^2/g). When NiO is impregnated on a support, the BET S.A. of the catalyst has been shown to be reduced compared to that of the support because NiO fills the pores of the support [34–36]. Figure S1 shows the nitrogen isotherm adsorption and desorption results of the catalysts. The type IV hysteresis loop is identified in all catalysts, which indicates that the catalysts have mesoporous structures [16]. The mesoporous structure of Ni-based catalysts is known to provide accessible Ni active centers and to stabilize Ni particles by confinement effect [18]. The dispersion of Ni from the prepared catalysts was calculated using the results of the H_2-chemisorption analysis and is shown in Table 1. A relatively high level of Ni dispersion was confirmed in the Ni/MG30, Ni/MG50, Ni/MG70, and Ni/MG90 catalysts compared to the Ni/MG10 catalyst. The Ni/MG30 catalyst showed the highest Ni dispersion (3.41%) among the prepared catalysts.

Table 1. Characteristics of Ni/MG catalysts with different MgO:Al_2O_3 ratios.

Catalyst	Support BET S.A. (m^2/g) [1]	Catalyst BET S.A. (m^2/g) [1]	Ni Dispersion (%) [2]	Crystallite Size of Ni^0 (nm) [3]
Ni/MG10	202.6	139.2	1.46	13.6
Ni/MG30	200.9	120.8	3.41	9.4
Ni/MG50	164.2	104.2	3.32	9.7
Ni/MG70	161.5	104.0	3.18	9.9
Ni/MG90	102.0	76.6	3.24	11.9

[1] Predicted from N_2 adsorption–desorption at −196 °C. [2] Predicted from H_2-chemisorption contemplating the Ni reduction degree. [3] Calculated from the Scherrer equation based on the XRD result.

Figure 1 demonstrates the XRD analysis results of the Ni/MG catalysts by diverse MgO:Al_2O_3 ratios. Peaks at 31.4, 37.0, 45.0, 59.7, and 65.5° were attributed to spinel $NiAl_2O_4$ (JCPDS #10-0339), and only the highest Al_2O_3-containing Ni/MG10 catalyst was identified. Peaks at 31.3, 36.9, 44.8, 59.4, and 65.2° were assigned to the spinel $MgAl_2O_4$ (JCPDS #21-1152) crystals, which can be identified with the increasing MgO content. The Ni/MG30 catalyst exhibited the strongest spinel $MgAl_2O_4$ peak intensity. The peaks at approximately 37, 43, 62, 75, and 79° were due to the cubic structure of unreduced NiO (JCPDS #04-0835) and MgO (JCPDS #65-0476). It was difficult to differentiate the positions of the NiO and MgO XRD diffraction peaks. As the MgO content increased, the intensity of the peak corresponding to the NiO-MgO solid solution produced by the interaction of NiO and MgO remaining after $MgAl_2O_4$ formation increased. All the reduced catalysts exhibited Ni^0 peaks at 44.5, 51.8, and 76.4°, which is an active phase during dry reforming of COG [14]. The crystallite size of Ni^0 was calculated from the peak (51.8°) assigned to the Ni^0 (2 0 0) plane using the Scherrer equation due to the peak overlap at the Ni^0 (1 1 1) plane peak, and the results are given in Table 1. In the prepared catalysts, the Ni/MG30 catalyst exhibited the smallest Ni crystal size (9.4 nm).

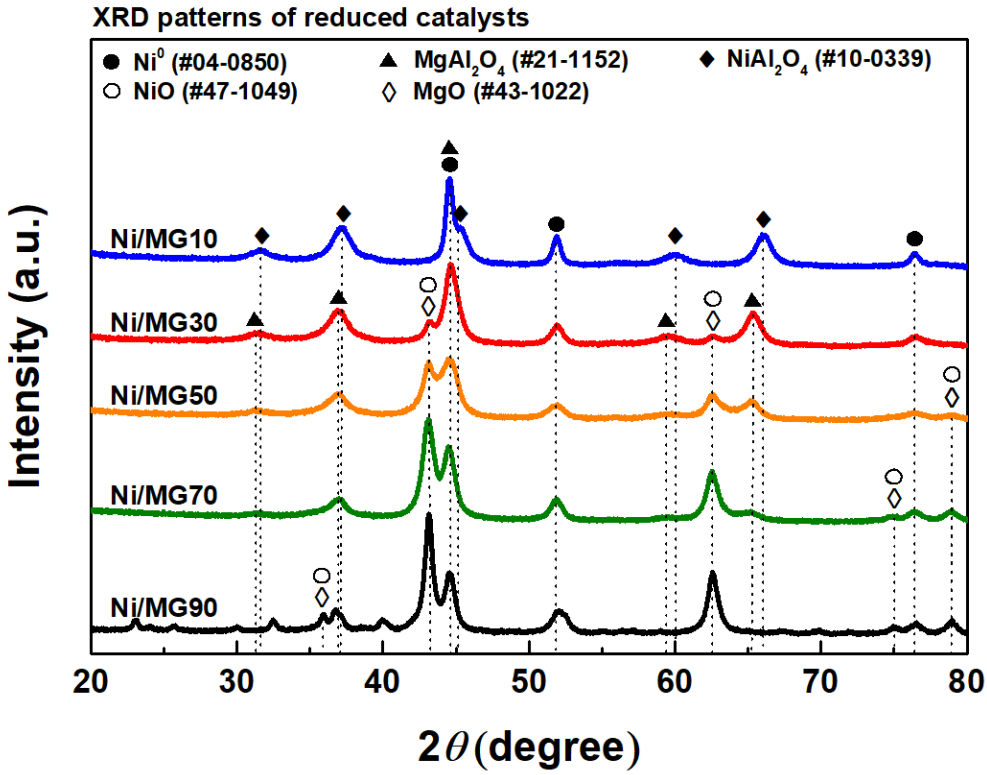

Figure 1. XRD results of Ni/MG catalysts with different MgO/Al_2O_3 ratios.

The oxidation/reduction properties of the catalysts were the primary factors influencing the catalyst activity in reforming reactions. TPR analysis was organized to understand the oxidation/reduction characteristics of the Ni/MG catalysts prepared with various MgO:Al_2O_3 ratios, and the results are shown in Figure 2. All prepared catalysts demonstrated large reduction peaks at 700–850 °C [27]. This was a peak owing to the reduction of the complex NiO species that interacted strongly with the support.

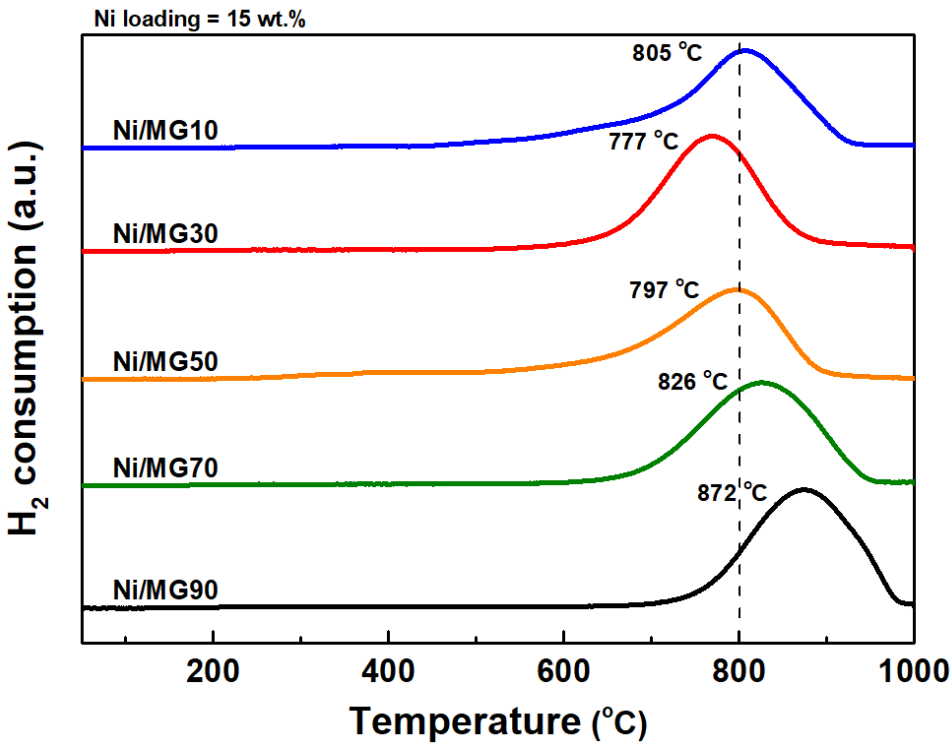

Figure 2. TPR results of Ni/MG catalysts with different MgO/Al_2O_3 ratios.

The composite NiO reduction peak of the Ni/MG catalyst at low temperature appeared with the following order: Ni/MG30 < Ni/MG10 < Ni/MG70 < Ni/MG50 < Ni/MG90. In the case of catalyst Ni/MG10, a high Al_2O_3 content was reported to be advantageous for forming a $NiAl_2O_4$ spinel structure; and when the $NiAl_2O_4$ spinel structure was formed, a reduced peak appeared at high temperature because of the strong interaction between NiO and Al_2O_3 [37–39]. On the other hand, Ni/MG30 was reduced at a lower temperature than the Ni/MG10 catalyst by the reduction of the NiO interacting with the $MgAl_2O_4$ spinel structure. However, with an increase in MgO, the reduction peak shifted to a higher temperature because of the strong interaction following the formation of the NiO-MgO solid solution [40,41].

Table 2 shows the results of the reduction degree analysis for Ni/MG catalysts under the reaction conditions. The reduction degree value is closely related to the number of active species in the reaction conditions. Therefore, the Ni/MG30 catalyst showing the highest value was expected to show the highest activity when applied to the dry reforming reaction.

Table 2. Reduction degree results of Ni/MG catalysts with different MgO/Al_2O_3 ratios.

Catalyst	Ni/MG10	Ni/MG30	Ni/MG50	Ni/MG70	Ni/MG90
Reduction degree (%) [1]	84	96	88	67	51

[1] Calculated from (H_2 consumption amount (800 °C)/H_2 consumption amount (1000 °C)) × 100.

CO_2-TPD analysis was used to examine the interaction of CO_2 with the synthesized Ni/MG catalyst. As shown in Figure 3, the Ni/MG catalyst exhibited a major desorption peak at 100–400 °C, which means that there was a strong basic site on the Ni/MG surface. According to the literature, the chemical properties of the support, especially the basicity, promoted the activation of CO_2 in the dry reforming reaction [42,43]. In addition, the conversion of both CH_4 and CO_2 was improved by increasing the removal rate of surface carbonaceous species, such as CH_x (x = 0–3), generated by the dehydrogenation of CH_4.

The high CO_2 adsorption capacity also improved the coke resistance of the catalyst [42,43]. Table 3 shows the amount of CO_2 desorbed by the prepared MG supports and Ni/MG catalysts. In the MG supports, as the ratio of MgO increased, the basicity of the support increased stepwise and then decreased again at the ratio of $MgO:Al_2O_3$ = 9:1. The Ni/MG30 catalyst exhibited the highest CO_2 adsorption amount (9.7 cm^3/gcat).

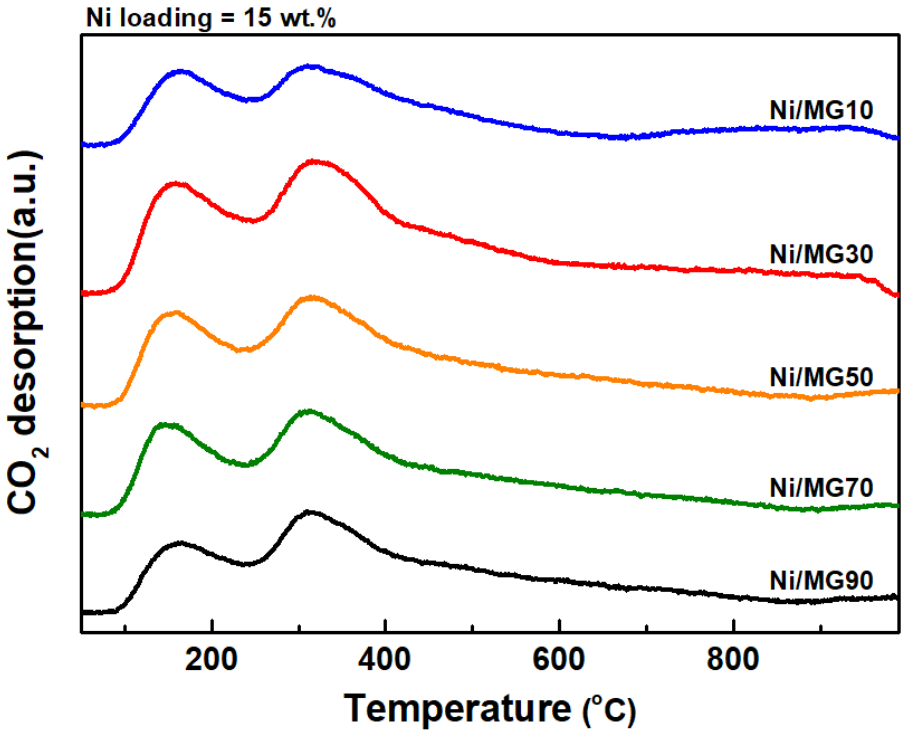

Figure 3. CO_2-TPD results of Ni/MG catalysts with different $MgO:Al_2O_3$ ratios.

Table 3. CO_2-TPD results of MG supports and Ni/MG catalysts with different $MgO:Al_2O_3$ ratios.

Catalyst	Support Desorbed CO_2 (cm^3/gcat)	Total Desorbed CO_2 (cm^3/gcat)
Ni/MG10	18.0	6.1
Ni/MG30	58.8	9.7
Ni/MG50	71.2	8.2
Ni/MG70	154.3	8.0
Ni/MG90	39.8	7.7

TEM and EDS mapping analysis was performed to confirm the supported state and composition of the prepared catalyst. Figure 4 shows the TEM and EDS mapping images of Ni/MG30 catalyst. The composition of the prepared Ni/MG catalyst followed (Ni: 13.28%, Mg: 28.01%, Al: 58.70%).

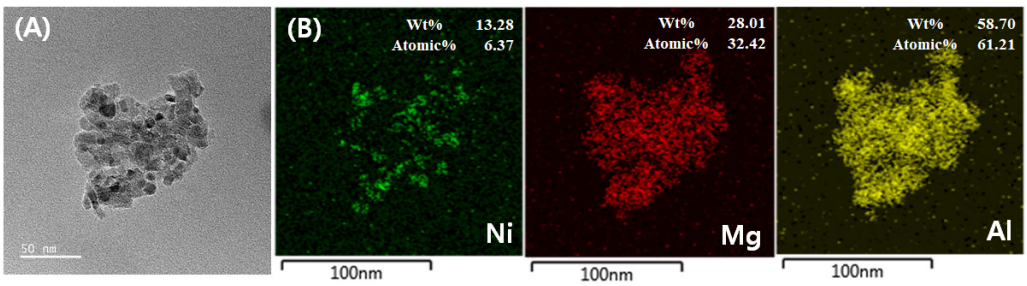

Figure 4. (**A**) TEM and (**B**) EDS mapping images of Ni/MG30 catalyst.

The elemental composition analysis of the Ni/MG catalyst prepared by inductively coupled plasma (ICP) was analyzed and is listed in Table S1. *In* ICP analysis results, for all the prepared catalysts, almost same catalyst composition was achieved, which is what we intended.

2.2. Reaction Results

Figure 5 shows the interrelationship between the physicochemical properties and the catalytic performance of the Ni/MG catalysts with various MgO:Al_2O_3 ratios. The BET S.A. of the prepared MgO-Al_2O_3 support decreased as the MgO content increased. In the case of the Ni/MG10 catalyst with the highest Al_2O_3 content in the support, the complex NiO reduction temperature increased, according to the formation of spinel $NiAl_2O_4$, and the catalyst showed low dispersion and a large crystallite size. As the MgO content increased, the complex NiO reduction temperature of complex NiO decreased according to the $MgAl_2O_4$ production. In the case of an excessive MgO content, a NiO-MgO solid solution, in which the excess MgO strongly interacted with NiO, was formed, the NiO reduction temperature increased to a high temperature, the dispersion decreased, and the crystallite size increased. The Ni/MG30 catalyst showed the highest CO_2 adsorption amount. As a result, the Ni/MG30 catalyst showed an appropriate correlation between complex NiO and the MgO-Al_2O_3, having the largest number of Ni^0 active sites.

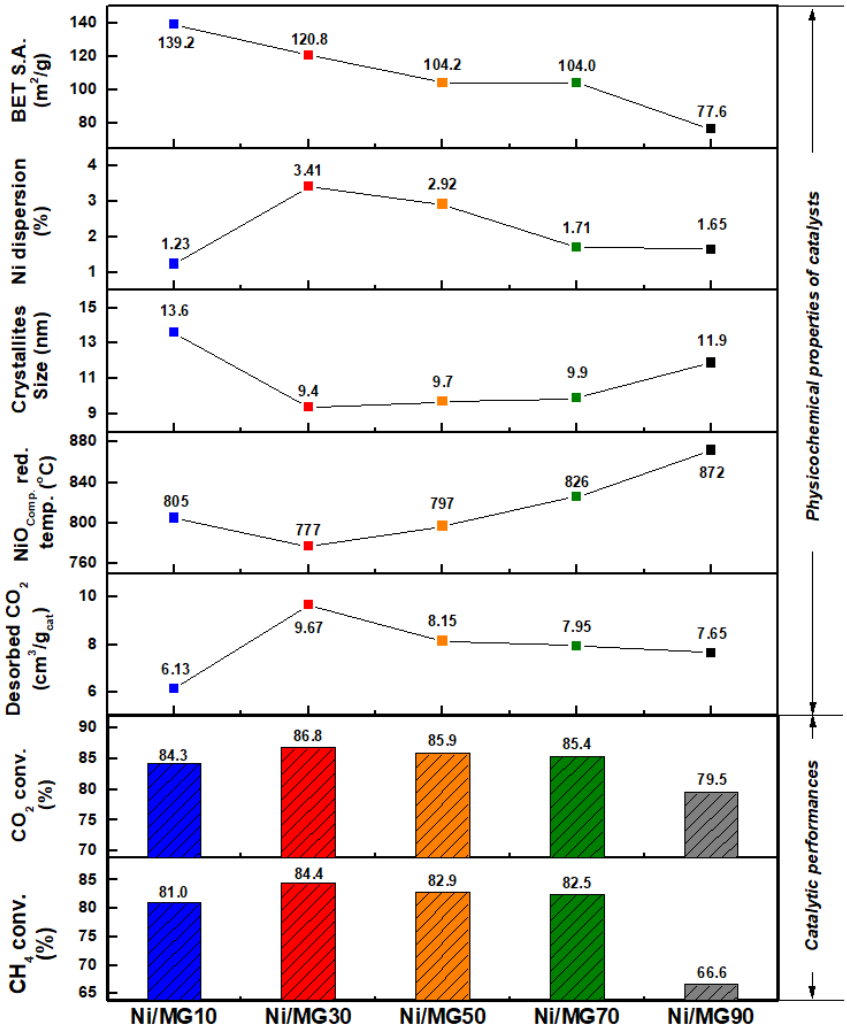

Figure 5. The relationships among the physicochemical properties of the catalysts and their catalytic performance.

Figure 6 shows the CH_4 conversion of Ni/MG catalysts. To screen the prepared catalyst performance, the reaction was performed under high GHSV conditions (GHSV = 1,500,000 h^{-1}) at 800 °C. As a result of the reaction, the Ni/MG30 catalyst had the highest CH_4 conversion (84.2%), and the Ni/MG90 catalyst had the lowest CH_4 conversion (66.6%). Even at high GHSV, all the prepared catalysts showed stable activity for 12 h.

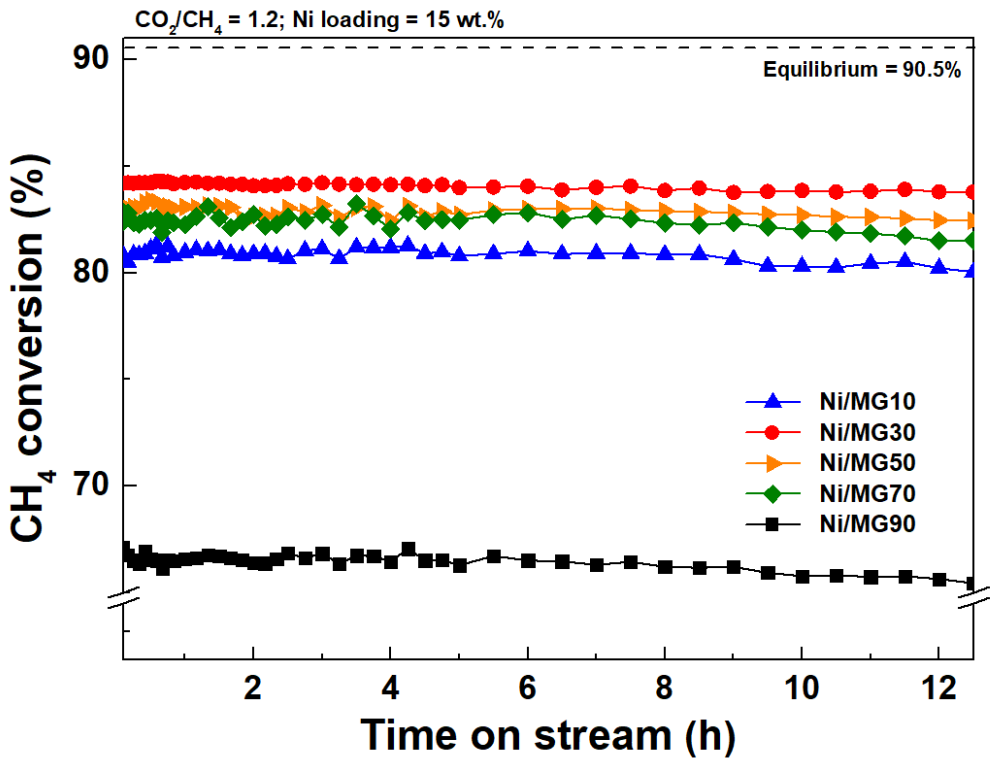

Figure 6. CH_4 conversion vs. time on stream for Ni/MG catalysts with diverse $MgO:Al_2O_3$ ratios (CO_2/CH_4 = 1.2; reaction temperature = 800 °C; GHSV =1,500,000 h^{-1}).

Figure 7 shows the CO_2 conversion of the Ni/MG catalysts. The CO_2 conversion was approximately 3% higher than the CH_4 conversion, and the H_2 yield was lower than the theoretical H_2 yield (H_2 yield (%): Ni/MG10 (77.6), Ni/MG30 (81.9), Ni/MG50 (79.8), Ni/MG70 (79.4), Ni/MG90 (53.9)). This was judged to be the result of the reverse water gas shift reaction (RWGS: $H_2 + CO_2 \rightarrow H_2O + CO$) during the dry reforming reaction [44]. The detailed reaction results, including the feed gas and outlet gas compositions, are shown in Table 4.

Table 4. CO_2 reforming of CH_4 using COG over Ni/MG30 catalyst (reaction results for 12 h).

Gas Composition (%) [1]						
Component	CH_4	CO_2	N_2	H_2	CO	Total
Reactant gas (COG) + CO_2	21.39	25.67	4.46	42.39	6.10	100.00
Product gas	2.65	2.68	3.53	55.27	35.87	100.00
Yield (%)		Conversion (%)		H_2/CO ratio		
H_2	CO	CH_4	CO_2	Reactant gas (COG) + CO_2		Product gas
64.0	83.2	84.4	86.8	6.95		1.54

[1] Evaluated by micro-GC.

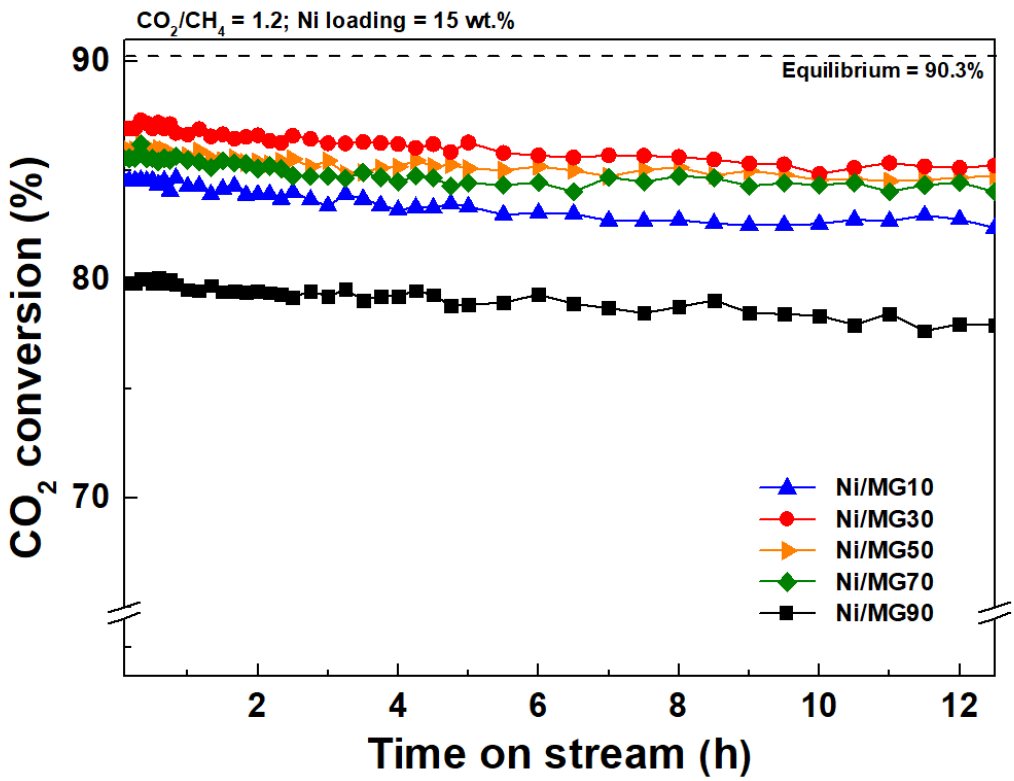

Figure 7. CO_2 conversion vs. time on stream over Ni/MG catalysts with diverse $MgO:Al_2O_3$ ratios (CO_2/CH_4 = 1.2; reaction temperature = 800 °C; GHSV = 1,500,000 h^{-1}).

3. Materials and Methods

3.1. Preparation of Catalysts

$MgO–Al_2O_3$ was prepared using a one-step coprecipitation method with different $MgO:Al_2O_3$ ratios as a support. $Mg(NO_3)_2·6H_2O$ (99%, Aldrich) and $Al(NO_3)_2·6H_2O$ (98%, Aldrich) were used as the precursors. KOH (95%, Samchun) was utilized as the precipitation agent. To support preparation, the precursors were stoichiometrically quantified and then dissolved in distilled water and a constant temperature at 80 °C. In a precipitation step, 15 wt% KOH solution was added at 0.8 mL/min to reach pH 10.5. The prepared solution was aged for 3 days and was then washed several times with distilled water to remove impurities, including the remaining K^+ and NO^{3-} ions. The precipitate was sufficiently dried at 100 °C to remove moisture. After that, it was calcined at 800 °C for 6 h. The Ni/MgO-Al_2O_3 catalyst was prepared through an impregnation method by supporting the $Ni(NO_3)_2·6H_2O$ (97%, Junsei) on the prepared MgO-Al_2O_3 support. The Ni loading was 15 wt. %, and the catalyst was dried at 100 °C and then calcined at 800 °C for 6 h. The finished Ni/MgO-Al_2O_3 catalyst was named according to the $MgO:Al_2O_3$ ratio, as indicated in Table 5.

Table 5. Ni/MgO-Al_2O_3 catalysts' naming convention.

$MgO:Al_2O_3$	Name
1:9	Ni/MG10
3:7	Ni/MG30
5:5	Ni/MG50
7:3	Ni/MG70
9:1	Ni/MG90

3.2. Catalyst Characterization

Transmission electron microscopy (TEM) images of the samples were obtained using a JEM-F200 (JEOL, Japan) microscope. Samples were blended with ethanol by using ultrasonication for 30 min. The prepared suspension was deposited on a grid. The elemental composition of prepared catalysts was analyzed by an inductively coupled, plasma-optical emission spectrometer (Varian, USA). The Brunauer–Emmett–Teller specific surface areas of the samples were investigated by the N_2 adsorption/desorption isotherms at −196 °C using an ASAP 2010 (Micromeritics, USA). X-ray diffraction (XRD) patterns were analyzed using a Rigaku Ultima IV diffractometer (RIGAKU, Japan). Detailed procedures of XRD and Ni^0 crystallite size calculation method were reported in our previous work [14]. H_2-chemisorption data were obtained using an Autochem 2920 (Micromeritics, US). The redox properties of the catalysts were evaluated via H_2 temperature-programmed reduction (H_2-TPR) using Autochem 2920. The reduction degree was estimated using the following equation, derived from the integration of the peak area below the TPR at 800 °C and 1000 °C:

$$\text{Reduction degree } (\%) = \frac{\text{H}_2 \text{ consumption amount } (800\ ^\circ\text{C})}{\text{H}_2 \text{ consumption amount } (1000\ ^\circ\text{C})} \times 100$$

H_2-chemisorption data were obtained using an Autochem 2920 (Micromeritics, USA). Detailed procedures of H_2-chemisorption were reported in our previous work [14]. CO_2 temperature-programmed desorption (CO_2-TPD) analyses were performed on an Autochem 2920 (Micromeritics, USA) instrument. In the pretreatment step, samples were fixed in a quartz U-tube and exposed with He at 300 °C for 10 min. The CO_2 adsorption step was performed in 10% CO_2/He for 30 min at 100 °C. Subsequently, physically adsorbed CO_2 was removed by purging with He for 1 h, and the treated samples were heated in a He flow from 100 to 1000 °C at a rate of 10 °C/min. The desorbed CO_2 was measured by a thermal conductivity detector (TCD).

3.3. Catalyst activity

The catalytic activity tests were performed under atmospheric pressure at 800 °C using a fixed-bed tubular quartz reactor with an inner diameter of 4 mm. The reactor temperature was monitored in real time and controlled by a temperature controller box. During the test procedure, 10 mg of the catalyst, 150 mg of the diluent, and a simulated coke oven gas (as the reactant gas: CH_4: 28.04%, CO_2: 2.56%, CO: 7.99%, H_2: 55.57%, N_2: 5.84%) were used, and CO_2 was supplied to increase the CO_2:CH_4 ratio to 1.2:1. The catalyst was loaded into the tubular quartz reactor, and a catalytic test was conducted at 800 °C. A high GHSV of 1.5 million h^{-1} was applied for 12 h to screen the activity. Before each measurement, the sample was reduced in situ at 800 °C for 3 h under 5% H_2/N_2 conditions. Each gas was controlled using an independent mass flow controller (MFC). Effluent gases from the reactor were chilled and allowed to pass through a moisture trap to remove the remaining H_2O. Then, the product gases were analyzed online using a micro-gas chromatograph (Agilent 3000, US). The CH_4, CO_2 conversions, H_2, CO yields, and H_2/CO ratio were defined as follows:

$$\text{CH}_4 \text{ conversion } (\%) = \frac{[\text{CH}_4]_{\text{in}} - [\text{CH}_4]_{\text{out}}}{[\text{CH}_4]_{\text{in}}} \times 100$$

$$\text{CO}_2 \text{ conversion } (\%) = \frac{[\text{CO}_2]_{\text{in}} - [\text{CO}_2]_{\text{out}}}{[\text{CO}_2]_{\text{in}}} \times 100$$

$$\text{H}_2 \text{ yield } (\%) = \frac{\text{H}_{2\text{out}} - \text{H}_{2\text{in}}}{2 \times \text{CH}_{4\text{in}}} \times 100$$

$$\text{CO yield } (\%) = \frac{\text{CO}_{\text{out}} - \text{CO}_{\text{in}}}{\text{CH}_{4\text{in}} + \text{CO}_{2\text{in}}} \times 100$$

$$H_2/CO \text{ ratio} = \frac{[H_2]_{out}}{[CO]_{out}}$$

where $[X]_{in}$ and $[X]_{out}$ are the inlet and outlet concentrations of X, respectively. In the same way, X_{in} and X_{out} are the inlet and outlet amounts of X, respectively.

4. Conclusions

To confirm the effect of the $MgO:Al_2O_3$ ratio in the Ni/MG catalyst for the dry reforming of COG, Ni/MG catalysts were prepared with varying $MgO:Al_2O_3$ ratios (1:9, 3:7, 5:5, 7:3, 9:1). The Ni/MG catalyst prepared with a $MgO:Al_2O_3$ ratio of 3:7 (Ni/MG30) showed the highest CH_4 and CO_2 conversion (84.2%, 86.9%) even at high GHSV (1.5 million h^{-1}) and was selected as the optimal production ratio.

In the case of the Ni/MG10 catalyst with the highest Al_2O_3 content in the support, the complex NiO reduction temperature was increased. In addition, it showed the formation of spinel $NiAl_2O_4$, with low dispersion and a large crystallite size. As the MgO content increased, the reduction temperature of complex NiO in Ni/MG30 catalyst decreased according to $MgAl_2O_4$ production. In the case of an excessive MgO content, a NiO-MgO solid solution, in which the excess MgO strongly interacted with NiO was formed, the NiO reduction temperature increased to a high temperature, the dispersion degree decreased, and the crystallite size increased. This resulted in the Ni/MG30 catalyst having the highest number of Ni^0 active sites. As a result, the Ni/MG30 catalyst showed an appropriate correlation between complex NiO and the $MgO\text{-}Al_2O_3$ and showed the highest basicity. Also, due to the high reducibility and dispersibility of the catalyst surface, it has the largest number of Ni^0 active sites. Consequently, the Ni/MG30 catalyst showed the highest catalytic activity between the prepared catalysts.

Supplementary Materials: The following are available online at https://www.mdpi.com/article/10.3390/catal11121468/s1. Figure S1: Adsorption/desorption isotherms of Ni/MG catalysts with different $MgO:Al_2O_3$ ratios. Table S1: The elemental composition of Ni/MG catalysts determined by ICP-OES.

Author Contributions: Conceptualization, formal analysis, H.-R.P., B.-J.K. and Y.-L.L.; writing—original draft preparation, visualization, validation, H.-R.P., methodology, S.-Y.A. and K.-J.K.; investigation, H.-R.P.; resources H.-R.P., B.-J.K. and Y.-L.L.; data curation, H.-R.P., B.-J.K., Y.-L.L., S.-Y.A., K.-J.K., G.-R.H. and S.-J.Y.; writing—review and editing, H.-R.P., B.-J.K., Y.-L.L., S.-Y.A., K.-J.K., G.-R.H., S.-J.Y., B.-H.J. and J.W.B.; supervision, H.-S.R.; project administration, H.-S.R.; funding acquisition, H.-S.R. All authors have read and agreed to the published version of the manuscript.

Funding: This work was supported by the "Next Generation Carbon Upcycling Project" (Project No. 2017M1A2A2044372) through the National Research Foundation (NRF) funded by the Ministry of Science and ICT, Korea.

Conflicts of Interest: The authors declare no conflict of interest.

References

1. *Adoption of the Paris Agreement, L.9*; UNFCCC: France, Paris, 2015; pp. 2–32.
2. Rogelj, J.; den Elzen, M.; Höhne, N.; Fransen, T.; Fekete, H.; Winkler, H.; Schaeffer, R.; Sha, F.; Riahi, K.; Meinshausen, M. Paris agreement climate proposals need a boost to keep warming well below 2 degrees Celsius. *Nature* **2016**, *534*, 631–639. [CrossRef]
3. *Energy Technology Perspectives 2016: Towards Sustainable Urban Energy Systems*; IEA: France, Paris, 2016; pp. 25–76.
4. Umar, M.; Ji, X.; Kirikkaleli, D.; Alola, A.A. The imperativeness of environmental quality in the United States transportation sector amidst biomass-fossil energy consumption and growth. *J. Clean. Prod.* **2021**, *285*, 124863. [CrossRef]
5. Al-mulali, U. Exploring the bi-directional long run relationship between energy consumption and life quality. *Renew. Sustain. Energy Rev.* **2016**, *54*, 824–837. [CrossRef]
6. Friedmann, S.J.; Fan, Z.; Tang, K. *Low-Carbon Heat Solutions for Heavy Industry: Sources, Options, and Costs Today*; CGEP, Columbia University: New York, NY, USA, 2019.
7. He, K.; Wang, L. A review of energy use and energy-efficient technologies for the iron and steel industry. *Renew. Sustain. Energy Rev.* **2017**, *70*, 1022–1039. [CrossRef]
8. Tian, S.; Jiang, J.; Zhang, Z.; Manovic, V. Inherent potential of steelmaking to contribute to decarbonization targets via industrial carbon capture and storage. *Nat. Commun.* **2018**, *9*, 1–8. [CrossRef] [PubMed]

9. Wang, P.; Ryberg, M.; Yang, Y.; Feng, K.; Kara, S.; Hauschild, M.; Chen, W.-Q. Efficiency stagnation in global steel production urges joint supply- and demand-side mitigation efforts. *Nat. Commun.* **2021**, *12*, 2066–2076. [CrossRef] [PubMed]
10. Naito, M.; Takeda, K.; Matsui, Y. Ironmaking technology for the last 100 years: Deployment to advanced technologies from introduction of technological know-how, and evolution to next-generation process. *ISIJ Int.* **2015**, *55*, 7–35. [CrossRef]
11. Uribe-Soto, W.; Portha, J.-F.; Commenge, J.-M.; Falk, L. A review of thermochemical processes and technologies to use steelworks off-gases. *Renew. Sustain. Energy Rev.* **2017**, *74*, 809–823. [CrossRef]
12. Park, J.E.; Koo, K.Y.; Jung, U.H.; Lee, J.H.; Roh, H.-S.; Yoon, W.L. Syngas production by combined steam and CO_2 reforming of coke oven gas over highly sinter-stable La-promoted $Ni/MgAl_2O_4$ catalyst. *Int. J. Hydrogen Energy* **2015**, *40*, 13909–13917. [CrossRef]
13. Aghaali, M.H.; Firoozi, S. Enhancing the catalytic performance of Co substituted $NiAl_2O_4$ spinel by ultrasonic spray pyrolysis method for steam and dry reforming of methane. *Int. J. Hydrogen Energy* **2021**, *46*, 357–373. [CrossRef]
14. Lee, Y.-L.; Kim, B.-J.; Park, H.-R.; Ahn, S.-Y.; Kim, K.-J.; Roh, H.-S. Customized Ni–MgO–Al_2O_3 catalyst for carbon dioxide reforming of coke oven gas: Optimization of preparation method and co-precipitation pH. *J. CO_2 Util.* **2020**, *42*, 101354–101362. [CrossRef]
15. Li, Z.; Jiang, B.; Wang, Z.; Kawi, S. High carbon resistant Ni@Ni phyllosilicate@SiO_2 core shell hollow sphere catalysts for low temperature CH_4 dry reforming. *J. CO_2 Util.* **2018**, *27*, 238–246. [CrossRef]
16. Karam, L.; Miglio, A.; Specchia, S.; Hassan, N.E.; Massiani, P.; Reboul, J. PET waste as organic linker source for the sustainable preparation of MOF-derived methane dry reforming catalysts. *Mater. Adv.* **2021**, *2*, 2750–2758. [CrossRef]
17. Liu, W.; Li, L.; Zhang, X.; Wang, Z.; Wang, X.; Peng, H. Design of Ni-ZrO_2@SiO_2 catalyst with ultra-high sintering and coking resistance for dry reforming of methane to prepare syngas. *J. CO_2 Util.* **2018**, *27*, 297–307. [CrossRef]
18. Jang, W.J.; Shim, J.O.; Kim, H.M.; Yoo, S.Y.; Roh, H.S. A review on dry reforming of methane in aspect of catalytic properties. *Catal Today* **2019**, *324*, 15–26. [CrossRef]
19. Li, X.; Li, D.; Tian, H.; Zeng, L.; Zhao, Z.J.; Gong, J. Dry reforming of methane over Ni/La_2O_3 nanorod catalysts with stabilized Ni nanoparticles. *Appl. Catal. B Environ.* **2017**, *202*, 683–694. [CrossRef]
20. Li, G.; Cheng, H.; Zhao, H.; Lu, X.; Xu, Q.; Wu, C. Hydrogen production by CO_2 reforming of CH_4 in coke oven gas over Ni–Co/$MgAl_2O_4$ catalysts. *Catal Today* **2018**, *318*, 46–51. [CrossRef]
21. Jang, W.J.; Kim, H.M.; Shim, J.O.; Yoo, S.Y.; Jeon, K.W.; Na, H.S.; Lee, Y.L.; Jeong, D.W.; Bae, J.W.; Nah, I.W.; et al. Key properties of Ni–MgO–CeO_2, Ni–MgO–ZrO_2, and Ni–MgO–$Ce_{(1-x)}Zr_{(x)}O_2$ catalysts for the reforming of methane with carbon dioxide. *Green Chem.* **2018**, *20*, 1621–1633. [CrossRef]
22. Ren, H.-P.; Ding, S.-Y.; Ma, Q.; Song, W.-Q.; Zhao, Y.-Z.; Liu, J.; He, Y.-M.; Tian, S.-P. The Effect of Preparation Method of Ni-Supported SiO_2 Catalysts for Carbon Dioxide Reforming of Methane. *Catalysts* **2021**, *11*, 1221. [CrossRef]
23. Talkhoncheh, S.K.; Haghighi, M. Syngas production via dry reforming of methane over Ni-based nanocatalyst over various supports of clinoptilolite, ceria and alumina. *J. Nat. Gas Sci. Eng.* **2015**, *23*, 16–25. [CrossRef]
24. Mozammel, T.; Dumbre, D.; Hubesch, R.; Yadav, G.D.; Selvakannan, P.R.; Bhargava, S.K. Carbon Dioxide Reforming of Methane over Mesoporous Alumina Supported Ni(Co), Ni(Rh) Bimetallic, and Ni(CoRh) Trimetallic Catalysts: Role of Nanoalloying in Imoriving the Stability and Nature of Coking. *Energy Fuels* **2020**, *34*, 16433–16444. [CrossRef]
25. Jang, W.J.; Jeong, D.W.; Shim, J.O.; Kim, H.M.; Han, W.B.; Bae, J.W.; Roh, H.S. Metal oxide (MgO, CaO, and La_2O_3) promoted Ni-$Ce_{0.8}Zr_{0.2}O_2$ catalysts for H_2 and CO production from two major greenhouse gases. *Renew. Energy* **2015**, *79*, 91–95. [CrossRef]
26. Han, J.W.; Park, J.S.; Choi, M.S.; Lee, H.J. Uncoupling the size and support effects of Ni catalysts for dry reforming of methane. *Appl. Catal. B Environ.* **2017**, *203*, 625–632. [CrossRef]
27. Margossian, T.; Larmier, K.; Kim, S.M.; Krumeich, F.; Fedorov, A.; Chen, P.; Müller, C.R.; Copéret, C. Molucularly Tailored Nickel Precursor and Support Yield a Stable Methane Dry Reforming Catalyst with Superior Metal Utilization. *J. Am. Chem. Soc.* **2017**, *139*, 6919–6927. [CrossRef] [PubMed]
28. Shen, D.; Huo, M.; Li, L.; Lyu, S.; Wang, J.; Wang, X.; Zhang, Y.; Li, J. Effect of alumina morphology on dry reforming of methane over Ni/Al_2O_3 catalysts. *Catal. Sci. Technol.* **2020**, *10*, 510–516. [CrossRef]
29. Shamskar, F.R.; Rezaei, M.; Meshkani, F. The influence of Ni loading on the activity and coke formation of ultrasound-assisted co-precipitated Ni–Al_2O_3 nanocatalyst in dry reforming of methane. *Int. J. Hydrogen Energy* **2017**, *42*, 4155–4164. [CrossRef]
30. Hou, Z.; Yokota, O.; Tanaka, T.; Yashima, T. Characterization of Ca-promoted Ni/-Al_2O_3 catalyst for CH_4 reforming with CO_2. *Appl. Catal. A Gen.* **2003**, *253*, 381–387. [CrossRef]
31. Alipoura, Z.; Rezaei, M.; Meshkani, F. Effect of Ni loadings on the activity and coke formation of MgO-modified Ni/Al_2O_3 nanocatalyst in dry reforming of methane. *J. Energy Chem.* **2014**, *23*, 633–638. [CrossRef]
32. Sengupta, S.; Deo, G. Modifying alumina with CaO or MgO in supported Ni and Ni–Co catalysts and its effect on dry reforming of CH_4. *J. CO_2 Util.* **2015**, *10*, 67–77. [CrossRef]
33. Guo, J.; Lou, H.; Zheng, X. The deposition of coke from methane on a $Ni/MgAl_2O_4$ catalyst. *Carbon* **2007**, *45*, 1314–1321. [CrossRef]
34. Zhang, Q.L.; Qiu, C.T.; Xu, H.D.; Lin, T.; Lin, Z.E.; Gong, M.C. Low-temperature selective catalytic reduction of NO with NH_3 over monolith catalyst of MnO_x/CeO_2-ZrO_2-Al_2O_3. *Catal. Today* **2011**, *175*, 171–176. [CrossRef]

35. Ko, J.H.; Park, S.H.; Jeon, J.K.; Kim, S.S.; Kim, S.C.; Kim, J.M.; Chang, D.; Park, Y.K. Low temperature selective catalytic reduction of NO with NH_3 over Mn supported on $Ce_{0.65}Zr_{0.35}O_2$ prepared by supercritical method: Effect of Mn precursors on NO reduction. *Catal. Today* **2012**, *185*, 290–295. [CrossRef]
36. Shen, B.; Zhang, X.; Ma, H.; Yao, Y.; Liu, T. A comparative study of Mn/CeO_2, Mn/ZrO_2 and $Mn/Ce\text{-}ZrO_2$ for low temperature selective catalytic reduction of NO with NH_3 in the presence of SO_2 and H_2O. *J. Environ. Sci.* **2013**, *25*, 791–800. [CrossRef]
37. Rynkowski, J.M.; Paryjczak, T.; Lenik, M. On the nature of oxidic nickel phases in $NiO/y\text{-}Al_2O_3$ catalysts. *Appl. Catal. A* **1993**, *106*, 73–82. [CrossRef]
38. Salagre, P.; Fierro, J.L.G.; Medina, F.; Sueiras, J.E. Characterization of nickel species on several y-alumina supported nickel sample. *J. Mol. Catal. A* **1996**, *106*, 125–134. [CrossRef]
39. Turlier, P.; Praliaud, H.; Moral, P.; Martin, G.A.; Dalmon, J.A. Influence of the nature of the support on the reducibility and catalytic properties of nickel: Evidence for a new type of metal support interaction. *Appl. Catal.* **1985**, *19*, 287–300. [CrossRef]
40. Xu, D.; Li, W.; Ge, Q.; Xu, H. A novel process for converting coalmine-drained methane gas to syngas over nickel–magnesia solid solution catalyst. *Fuel Process. Technol.* **2005**, *86*, 995–1006. [CrossRef]
41. Arena, F.; Frusteri, F.; Giordano, N. Temperature-programmed Reduction Study of NiO-MgO Interactions in Magnesia-supported Ni Catalysts and NiO-MgO Physical Mixture. *J. Chem. Soc. Faraday Trans.* **1990**, *86*, 2663–2669. [CrossRef]
42. Wang, Y.; Ohtsuka, Y. Mn-based binary oxides as catalysts for the conversion of methane to C2 hydrocarbons with carbon dioxide as oxidant. *Appl. Catal. A* **2001**, *219*, 183–193. [CrossRef]
43. Zangeneh, F.T.; Sahebdelfar, S.; Ravanchi, T.M. Conversion of carbon dioxide to valuable petrochemicals: An approach to clean development mechanism. *J. Nat. Gas Chem.* **2011**, *20*, 219–231. [CrossRef]
44. Roh, H.-S.; Potdar, H.S.; Jun, K.-W.; Kim, J.-W.; Oh, Y.-S. Carbon dioxide reforming of methane over Ni incorporated into $Ce\text{–}ZrO_2$ catalysts. *Appl. Catal. A* **2004**, *276*, 231–239. [CrossRef]